

---

# HyNet: Local Descriptor with Hybrid Similarity Measure and Triplet Loss

---

Yurun Tian<sup>1</sup>   Axel Barroso-Laguna<sup>1</sup>   Tony Ng<sup>1</sup>   Vassileios Balntas<sup>2</sup>  
 Krystian Mikolajczyk<sup>1</sup>

<sup>1</sup> Imperial College London

<sup>2</sup> Facebook Reality Labs

{yurun.tian, axel.barroso17, tony.ng14, k.mikolajczyk}@imperial.ac.uk  
 vassileios@fb.com

## Abstract

Recent works show that local descriptor learning benefits from the use of  $L_2$  normalisation, however, an in-depth analysis of this effect lacks in the literature. In this paper, we investigate how  $L_2$  normalisation affects the back-propagated descriptor gradients during training. Based on our observations, we propose HyNet, a new local descriptor that leads to state-of-the-art results in matching. HyNet introduces a hybrid similarity measure for triplet margin loss, a regularisation term constraining the descriptor norm, and a new network architecture that performs  $L_2$  normalisation of all intermediate feature maps and the output descriptors. HyNet surpasses previous methods by a significant margin on standard benchmarks that include patch matching, verification, and retrieval, as well as outperforming full end-to-end methods on 3D reconstruction tasks.

## 1 Introduction

Local feature detectors and descriptors play a key role in many computer vision tasks such as 3D reconstruction or visual localisation. Recently, joint detection and description [45, 29, 9, 10, 32, 22, 25, 13] has drawn significant attention. Despite the alluring idea of the end-to-end detection and description, the classic two-stage strategy withstood years of tests in many computer vision tasks and still gives a competitive performance in standard benchmarks [5, 1, 36, 18]. Moreover, customised matchers [27, 34, 33, 4, 35] have also contributed to boosting the matching performance, where the time complexity is critical. Despite the progress in end-to-end methods, the two-stage process still deserves attention since it often leads to competitive results in the overall matching system [41].

Deep descriptors [38, 2, 40, 26, 19, 15, 41, 47] have shown superiority over hand-crafted ones [23, 44] in different tasks [1, 18, 5, 36]. Current works mainly focus on improving the loss function or the sampling strategy. L2-Net [40] introduces a progressive batch sampling with an N-Pair loss. HardNet [26] uses a simple yet effective hard negative mining strategy, justifying the importance of the sampling. Other than contrastive or triplet loss, DOAP [15] employs a retrieval based ranking loss. GeoDesc [24] integrates geometry constraints from multi-view reconstructions to benefit the training. Besides the first-order optimisation, SOSNet [41] shows that second-order constraints further improve the descriptors.

It has been widely observed that  $L_2$  normalisation of the descriptors leads to consistent improvements. Methods such as [40, 26, 15, 11, 41, 49, 47] which  $L_2$  normalised descriptors, significantly outperform early unnormalised descriptors [38, 2]. Moreover, even hand-crafted descriptors can be improved with  $L_2$  normalisation [1]. All such observations indicate that

descriptors are better distinguished by their vector directions rather than the magnitudes ( $L_2$  norms), where similar conclusions can also be found in other feature embedding tasks [43, 8, 21].

We therefore analyse the impact of  $L_2$  normalisation on learning from the gradients perspective. Since the gradients for each layer are generated via the chain rule [14], we analyse them at the beginning of the chain, where they are generated by the given similarity measure. Our intuition is that the gradient direction should benefit the optimisation of descriptor directions, while the gradient magnitude should be adaptive to the level of hardness of the training samples. Consequently, HyNet is introduced to make better use of the gradient signals in terms of direction and magnitude.

Despite the evolving design of loss function, triplet loss is still employed in state-of-the-art local descriptors [26, 41]. Furthermore, triplet loss has also earned noticeable popularity in various embedding tasks, *e.g.* face recognition [37, 30] and person re-identification [6, 16]. An interesting observation in [28] indicates that the improvements from the classic contrastive and triplet loss are marginal. In this work, we further show that state-of-the-art local descriptor can be learned by triplet loss with a better designed similarity measure.

Specifically, we propose: 1) a hybrid similarity measure that can balance the gradient contributions from positive and negative samples, 2) a regularisation term which provides suitable constraints on descriptor norms, and 3) a new network architecture that is able to  $L_2$  normalise the intermediate feature maps.

## 2 Gradient Analysis

In this section, we explore how the widely used inner product and  $L_2$  distance provide gradients for training normalised and unnormalised descriptors.

### 2.1 Preliminaries

We denote  $\mathcal{L}(s(\mathbf{x}, \mathbf{y}))$  as the loss for a descriptor pair  $(\mathbf{x}, \mathbf{y})$ , where  $s(\cdot, \cdot)$  is a similarity measure. Whether  $(\mathbf{x}, \mathbf{y})$  are positive (matching) or negative (non-matching), the gradients with respect to the descriptors are calculated as:

$$\frac{\partial \mathcal{L}}{\partial \mathbf{x}} = \frac{\partial \mathcal{L}}{\partial s} \frac{\partial s}{\partial \mathbf{x}}, \quad \frac{\partial \mathcal{L}}{\partial \mathbf{y}} = \frac{\partial \mathcal{L}}{\partial s} \frac{\partial s}{\partial \mathbf{y}}, \quad (1)$$

where  $(\mathbf{x}, \mathbf{y})$  are omitted for clarity. Importantly, the gradients for learnable weights of a network are derived in Eqn.(1) at the beginning of the chain, and play a key role during training. Note that  $\frac{\partial \mathcal{L}}{\partial s}$  is a scalar, while the direction of the gradient is determined by the partial derivatives of  $s$ . We consider the two most commonly used similarity measures, namely inner product and  $L_2$  distance, for descriptors with and without  $L_2$  normalisation:

$$s_I = \mathbf{x}^T \mathbf{y}, \quad \bar{s}_I = \frac{\mathbf{x}^T \mathbf{y}}{\|\mathbf{x}\| \|\mathbf{y}\|}, \quad s_L = \|\mathbf{x} - \mathbf{y}\|, \quad \bar{s}_L = \left\| \frac{\mathbf{x}}{\|\mathbf{x}\|} - \frac{\mathbf{y}}{\|\mathbf{y}\|} \right\|, \quad (2)$$

where  $\|\cdot\|$  denotes the  $L_2$  norm ( $\|\mathbf{x}\| = \sqrt{\sum \mathbf{x}_i^2}$ ).  $\bar{s}_I$  and  $\bar{s}_L$  are similarity measures<sup>1</sup> for normalised descriptors while  $s_I$  and  $s_L$  are for the unnormalised ones. Note that we consider  $L_2$  normalisation as a part of the similarity measure. We then obtain the partial derivatives:

$$\begin{aligned} \frac{\partial s_I}{\partial \mathbf{x}} &= \mathbf{y}, \quad \frac{\partial s_I}{\partial \mathbf{y}} = \mathbf{x}, \quad \frac{\partial s_L}{\partial \mathbf{x}} = \frac{1}{s_L}(\mathbf{x} - \mathbf{y}), \quad \frac{\partial s_L}{\partial \mathbf{y}} = \frac{1}{s_L}(\mathbf{y} - \mathbf{x}), \\ \frac{\partial \bar{s}_I}{\partial \mathbf{x}} &= \frac{1}{\|\mathbf{x}\| \|\mathbf{y}\|}(\mathbf{y} - \frac{\mathbf{x}^T \mathbf{y}}{\|\mathbf{x}\|^2} \mathbf{x}), \quad \frac{\partial \bar{s}_I}{\partial \mathbf{y}} = \frac{1}{\|\mathbf{x}\| \|\mathbf{y}\|}(\mathbf{x} - \frac{\mathbf{x}^T \mathbf{y}}{\|\mathbf{y}\|^2} \mathbf{y}), \\ \frac{\partial \bar{s}_L}{\partial \mathbf{x}} &= \frac{1}{s_L \|\mathbf{x}\| \|\mathbf{y}\|}(\frac{\mathbf{x}^T \mathbf{y}}{\|\mathbf{x}\|^2} \mathbf{x} - \mathbf{y}), \quad \frac{\partial \bar{s}_L}{\partial \mathbf{y}} = \frac{1}{s_L \|\mathbf{x}\| \|\mathbf{y}\|}(\frac{\mathbf{x}^T \mathbf{y}}{\|\mathbf{y}\|^2} \mathbf{y} - \mathbf{x}). \end{aligned} \quad (3)$$

In the following sections we analyse the above gradients in terms of directions and magnitudes.

---

<sup>1</sup>To ensure consistency, we refer to the  $L_2$  distance also as a similarity measure even though it measures the inverse similarity.

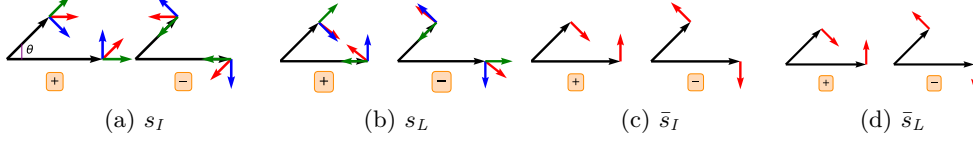


Figure 1: Gradient descent directions derived in Eqn. 3, with + and - for positive and negative pairs.  $\theta$  is the angle between the descriptors. **Black** arrows: descriptors before  $L_2$  normalisation. **Red** arrow: gradient descent direction from  $\Delta$ . **Green** arrow: parallel component from  $\Delta_{\parallel}$ . **Blue** arrows: orthogonal component from  $\Delta_{\perp}$ . Note that  $\Delta = \Delta_{\perp}$  for (c)  $\bar{s}_I$  and (d)  $\bar{s}_L$ . The vector lengths are irrelevant in this figure. Better viewed in colour.

## 2.2 Gradient Direction

Optimal gradient direction is the key for convergence, *i.e.*, a learning process will not converge given incorrectly directed gradients, regardless of the learning rate. We denote  $\Delta = \Delta_{\parallel} + \Delta_{\perp}$ , where  $\Delta$  is the gradient direction,  $\Delta_{\parallel}$  and  $\Delta_{\perp}$  are the parallel and orthogonal components, respectively. According to Eqn. (3), we obtain  $|\Delta_{\parallel}| = \mathbf{x}^T \frac{\partial \bar{s}_I}{\partial \mathbf{x}} = 0$ , and similarly for  $\mathbf{y}^T \frac{\partial \bar{s}_I}{\partial \mathbf{y}} = 0$ ,  $\mathbf{x}^T \frac{\partial \bar{s}_L}{\partial \mathbf{x}} = 0$ , and  $\mathbf{y}^T \frac{\partial \bar{s}_L}{\partial \mathbf{y}} = 0$ , *i.e.*, gradients are always orthogonal to the descriptors, indicating that  $L_2$  normalised descriptors only have  $\Delta_{\perp}$ . Meanwhile, unnormalised descriptors both components non-zero. For better understanding, we illustrate 2D descriptors and the corresponding gradient descent directions (negative gradient direction) in Fig. 1, where  $\theta$  is the angle between descriptors. Specifically,  $\Delta_{\parallel}$  modifies the descriptor magnitude ( $L_2$  norms), while  $\Delta_{\perp}$  updates the descriptor direction. However, since descriptor magnitudes can be harmful for matching (see Sec. 1), the training should focus on the optimisation of the descriptor directions, which can be achieved with  $L_2$  normalised descriptors. An interesting question is whether it is possible to make a better use of  $\Delta_{\parallel}$ . We address this problem in Sec. 3.1 and show that detailed analysis leads to training constraints that improve the performance.

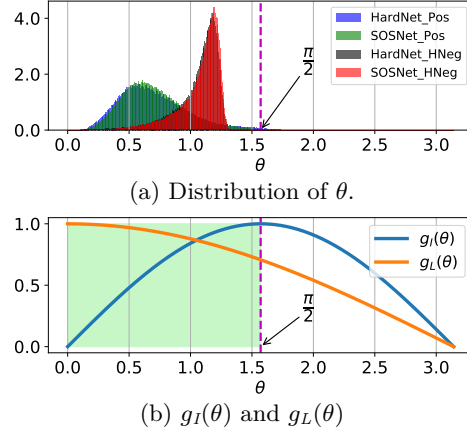


Figure 2: Gradient magnitude and distribution of  $\theta$ . Note that from Eqn. 4 the gradients are periodic functions with a period of  $\pi$ .

## 2.3 Gradient Magnitude

The training gradients should have not only the optimal directions but also the properly scaled magnitudes. The magnitude should be adapted to the level of 'hardness' of the training samples, *i.e.*, hard samples should receive a stronger update over easy ones.

We focus on  $L_2$  normalised descriptors whose gradients have optimal directions. We denote  $\mathbf{u} = \frac{\mathbf{x}}{\|\mathbf{x}\|}$  and  $\mathbf{v} = \frac{\mathbf{y}}{\|\mathbf{y}\|}$  as two descriptors normalised with  $L_2$ . With a slight abuse of notation, we use  $s(\theta)$  and  $g(\theta)$  to represent the similarity measure and gradient magnitude, respectively, with angle  $\theta$  between  $\mathbf{u}$  and  $\mathbf{v}$ :

$$\begin{aligned} s_I(\theta) &= \mathbf{u}^T \mathbf{v} = \cos \theta, & g_I(\theta) &= \left| \frac{d\mathbf{u}^T \mathbf{v}}{d\theta} \right| = |\sin \theta|, \\ s_L(\theta) &= \|\mathbf{u} - \mathbf{v}\| = \sqrt{2(1 - \cos \theta)}, & g_L(\theta) &= \left| \frac{d\|\mathbf{u} - \mathbf{v}\|}{d\theta} \right| = \left| \frac{\sin \theta}{\sqrt{2(1 - \cos \theta)}} \right|, \end{aligned} \quad (4)$$

where  $\theta = \arccos \mathbf{u}^T \mathbf{v}$ , and  $|\cdot|$  denotes the absolute value.

We analyse the similarities and gradient magnitudes from Eqn. (4) in the real descriptor space during training. Fig. 2(a) shows the distribution of  $\theta$  from 512K descriptor pairs, where the number of positive and negative pairs is 50% each. Specifically, following the hard negative mining strategy of [26], we sample 512 triplets (one positive pair and one negative) from each of the 1K randomly constructed batches of size 1024. Fig. 2(a) shows the  $\theta$  distribution of HardNet and SOSNet in training, *i.e.*, both models are trained and tested on *Liberty*. As shown, almost all hard negatives and positives have  $\theta$  in the range  $[0, \pi/2]$ . Worth noting that easy negatives may have  $\theta > \pi/2$ , however, sampling hard negatives only, has been proven to be effective [26]. Similarly, we observe how  $g_I(\theta)$  and  $g_L(\theta)$  behave in range  $[0, \pi/2]$ , which is highlighted in Fig. 2(b). The gradients differ, *i.e.*,  $g_I(\theta)$  is monotonically increasing while  $g_L(\theta)$  is decreasing. It indicates that  $g_I(\theta)$  is more beneficial for the optimisation of positives, since hard positives (large  $\theta \rightarrow \pi/2$ ), generate large gradients compared to easy positives (small  $\theta$ ). In contrast,  $g_L(\theta)$  favours negatives, as hard negatives (small  $\theta$ ) generate large updates compared to the easy negatives (large  $\theta$ ). These observations lead to the conclusion that neither the inner product nor the  $L_2$  on its own can balance the optimisation with positives and negatives.

It is also worth noting that according to Eqn. (1), the overall gradient magnitude is further weighted by  $\frac{\partial \mathcal{L}}{\partial s}$ , which means a better form of  $\mathcal{L}$  may alleviate the inherent flaws of  $g_I(\theta)$  and  $g_L(\theta)$ . Consequently, in Sec. 3.2 we show that a carefully designed similarity measure leads to the state-of-the-art performance with the standard triplet loss.

### 3 Method

Building upon the analysis from the previous section, we propose to improve the descriptor learning by 1) introducing a regularisation term that provides a beneficial  $\Delta_{\parallel}$ , 2) a hybrid similarity measure that can strike a balance between the contribution of positives and negatives to the gradient update, 3) a new network architecture that normalises the intermediate feature maps with affine  $L_2$  such that they are optimised in their directions rather than the magnitudes.

#### 3.1 $L_2$ Norm Regularisation

Section 2.2 shows that  $L_2$  normalisation excludes parallel gradients  $\Delta_{\parallel}$ , *i.e.*, there are no constraints on the descriptor norms which can vary with scaling of image intensities. Intuitively, a possible way of making positive contributions from  $\Delta_{\parallel}$  to the optimisation is to introduce the following constraint before the  $L_2$  normalisation:

$$R_{L_2} = \frac{1}{N} \sum_{i=1}^N (\|\mathbf{x}_i\| - \|\mathbf{x}_i^+\|)^2. \quad (5)$$

where  $\mathbf{x}_i$  and  $\mathbf{x}_i^+$  are a positive pair of descriptors before  $L_2$  normalisation. As a regularisation term,  $R_{L_2}$  drives the network to be robust to image intensity changes, *e.g.*, caused by different illuminations.

#### 3.2 Hybrid Similarity Measure and Triplet Loss

The standard triplet loss is defined as:

$$\mathcal{L}_{Triplet} = \frac{1}{N} \sum_{i=1}^N \max(0, m + s(\theta_i^+) - s(\theta_i^-)), \quad (6)$$

where  $m$  is the margin.  $\theta_i^+$  and  $\theta_i^-$  are the angles for the positive and negative pairs of the  $i$ -th descriptor triplet, *i.e.*, the angles between the anchor descriptor and its positive and negative samples.

Remarkable improvements have been made by modifying the standard triplet loss [26, 46, 48, 12, 48]. From the gradient perspective, when the margin constraint in Eqn. (6) is not satisfied, we obtain  $\frac{\partial \mathcal{L}_{Triplet}}{\partial s(\theta_i^+)} = \frac{\partial \mathcal{L}_{Triplet}}{\partial s(\theta_i^-)} = 1$ , otherwise 0. Hence, according to Eqn. (1),  $\frac{\partial s(\theta_i^+)}{\partial \theta_i^+}$



Figure 3: HyNet architecture. It consists of 7 convolutional layers which all but the last are followed by a FRN [39] normalisation and a TLU non-linearity [39].

and  $\frac{\partial s(\theta_i^-)}{\partial \theta_i^-}$  is directly related to the gradient magnitude. As discussed in Sec. 2.3,  $s_I$  and  $s_L$  lead to significantly different updates from the positive and negative examples. Intuitively, a direct solution would be to use  $s_I$  for positives while  $s_L$  for negatives, however, as we show in Sec. 5 this strategy is not optimal. Instead, we propose a hybrid similarity measure that combines the inner product  $s_I$  and the  $L_2$   $s_L$  :

$$s_H(\theta) = \frac{1}{Z} [\alpha(1 - s_I(\theta)) + s_L(\theta)], \quad (7)$$

where  $\alpha$  is a scalar ranging from 0 to  $+\infty$ , and  $Z$  is the normalising factor ensuring the gradient has the maximum magnitude of 1.

Finally, our overall loss function is defined as:

$$\mathcal{L}_{Triplet} = \frac{1}{N} \sum_{i=1}^N \max(0, m + s_H(\theta_i^+) - s_H(\theta_i^-)) + \gamma R_{L_2} \quad (8)$$

with  $\gamma$  as a regularisation parameter and  $\alpha$  balancing the contributions from  $s_I$  and  $s_L$ . Optimal  $\alpha$  can be found by a grid search which is discussed in Sec. 5.

### 3.3 Network Architecture

Our intuition for designing the network architecture is based on the analysis in Sec. 2.2 that, similarly to the output descriptors,  $L_2$  normalisation needs to be applied to the intermediate feature maps. However, we found that additional affine scaling of normalised maps has a positive effect on the output descriptors. To this end, we apply the Filter Response Normalisation (FRN) [39], which has recently been proposed and shown promising results in the classification task. Specifically, FRN normalises each layer of feature maps by:

$$\hat{\mathbf{f}}_i = \gamma \sqrt{N} \frac{\mathbf{f}_i}{\|\mathbf{f}_i\|} + \beta, \quad (9)$$

where  $\gamma$  and  $\beta$  are learned parameters,  $\mathbf{f}_i$  is the flattened feature map of the  $i$ -th channel and  $N$  is the number of pixels. As argued in [39] the gradients w.r.t  $\mathbf{f}_i$  are always orthogonal, hence as discussed in Sec. 2.2, the training can focus on optimising the directions of feature vectors.

Our HyNet architecture is based on L2-Net [40], which consists of seven convolutional layers and outputs 128-dimensional descriptors. As shown in Fig 3, all Batch Normalisation (BN) [17] layers, except the last one before the final  $L_2$  normalisation in the original L2-Net, are replaced with FRN layers. Moreover, as recommended in [39], each FRN is followed by the Thresholded Linear Unit (TLU) instead of the conventional ReLU. Thus, HyNet has the same number of convolutional weights as HardNet [26] and SOSNet [41].

## 4 Experiment

Our novel architecture and training is implemented in PyTorch [31]. The network is trained for 200 epochs with a batch size of 1024 and Adam optimizer [20]. Training starts from scratch, and the threshold  $\tau$  in TLU for each layer is initialised with  $-1$ . We set  $\alpha = 2$  and  $\gamma = 0.1$ . In the following experiments, HyNet is compared with recent deep local descriptors [2, 40, 26, 41] as well as end-to-end methods [9, 10, 32] on three standard benchmarks [5, 1, 36].

#### 4.1 UBC

UBC dataset [5] consists of three subsets-scenes, namely *Liberty*, *Notredame* and *Yosemite*. The benchmark is focused on the patch pair verification task, *i.e.*, whether the match is positive or negative. Following the evaluation protocol [5], models are trained on one subset and tested on the other two. In Table 1, we report the standard measure of false positive rate at 95% recall (FPR@95) [5] on six train and test splits. We can observe that, while the performance is nearly saturated, HyNet still shows remarkable improvements over previous methods.

Train	ND	YOS	LIB	YOS	LIB	ND	Mean
Test	LIB		ND		YOS		
SIFT [23]	29.84		22.53		27.29		26.55
TFeat [2]	7.39	10.13	3.06	3.80	8.06	7.24	6.64
L2-Net [40]	2.36	4.70	0.72	1.29	2.57	1.71	2.23
HardNet [26]	1.49	2.51	0.53	0.78	1.96	1.84	1.51
DOAP [15]	1.54	2.62	0.43	0.87	2.00	1.21	1.45
SOSNet [41]	1.08	2.12	0.35	0.67	1.03	<b>0.95</b>	1.03
<b>HyNet</b>	<b>0.89</b>	<b>1.37</b>	<b>0.34</b>	<b>0.61</b>	<b>0.88</b>	0.96	<b>0.84</b>

Table 1: Patch verification performance on the UBC phototour dataset. Numbers denote false positive rates at 95% recall(FPR@95). ND: Notredame, LIB: Liberty, YOS: Yosemite.

#### 4.2 HPatches

HPatches dataset [1] evaluates three tasks, patch verification, patch retrieval, and image matching for viewpoint and illumination changes between local patches. Based on different levels of geometric noise, the results are divided into 3 groups: *easy*, *hard*, and *tough*. We show the results in Fig. 4, where all models are trained on *Liberty*, which is the protocol proposed in [1]. HyNet improves the MAP from the previous state-of-the-art SOSNet [41] by a large margin, *i.e.*, **0.89%**, **2.35%**, and **1.75%** for the three tasks. Note that the improvement of SOSNet over its predecessor HardNet [26] was 0.03%, 0.96%, and 1.14% at the time of its publication.

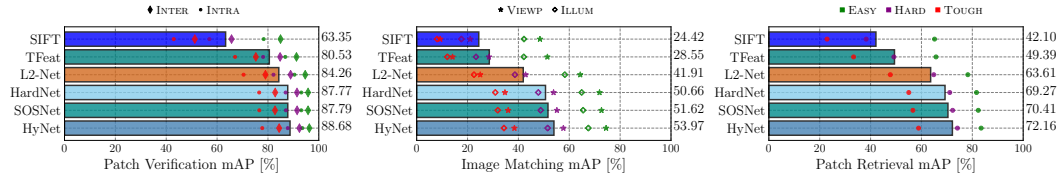


Figure 4: Results on test set ‘a’ of HPatches [1]. HyNet outperforms the state-of-the-art SOSNet [41] and other local image descriptors in all metrics on this benchmark.

#### 4.3 ETH

ETH SfM benchmark [36] evaluates local descriptors in the task of Structure from Motion (SfM) for outdoor scenes. To quantify the SfM quality, in Table 2, we follow the protocol from [36] and report the number of registered images, reconstructed sparse and dense points, mean track length, and mean reprojection error. First, we compare HyNet with HardNet [26] and SOSNet [41] by using the same local patches extracted from DoG detector, which is presented above the dashed lines. Since the detector is fixed, the results reflect the performance of the descriptors. To ensure a fair comparison, HardNet, SOSNet, and HyNet are all trained on *Liberty* from UBC dataset [5]. In this benchmark, HyNet exhibits significant superiority by registering more images for large scenes and reconstructing more sparse points, while the results for the other metrics are on par with top performing descriptors. Next, we compare HyNet to the recent end-to-end methods, namely SuperPoint [9], D2-Net [10] and R2D2 [32]. DoG+HyNet shows significantly better performance on larger scenes, for example, *Madrid Metropolis* and *Gendarmenmarkt*, where it gives over 50% more of reconstructed sparse points in 3D. Note that in the SfM task, the number of registered images and reconstructed points is crucial for the quality of 3D models. Moreover, results also show that HyNet generalises

well to different patches provided by the state-of-the-art detector Key.Net [3], where the average track length is increased for a number of scenes.

		#Reg. Images	#Sparse Points	#Dense Points	Track Length	Reproj. Error
<b>Herzjesu 8 images</b>	SIFT (11.3K)	8	7.5K	241K	4.22	<b>0.43px</b>
	DoG+HardNet	8	8.7K	239K	4.30	0.50px
	DoG+SOSNet	8	8.7K	239K	4.31	0.50px
	DoG+HyNet	8	<b>8.9K</b>	<b>246K</b>	<b>4.32</b>	0.52px
	SuperPoint (6.1K)	8	5K	244K	4.47	0.79px
	D2-Net (13.1K)	8	<b>13K</b>	221K	2.87	1.37px
	R2D2 (12.1K)	8	10K	244K	4.48	1.04px
	Key.Net+HyNet (11.9K)	8	9.4K	<b>246K</b>	<b>5.24</b>	<b>0.69px</b>
<b>Fountain 11 images</b>	SIFT (11.8K)	11	14.7K	292K	4.79	<b>0.39px</b>
	DoG+HardNet	11	16.3K	303K	4.91	0.47px
	DoG+SOSNet	11	16.3K	<b>306K</b>	4.92	0.46px
	DoG+HyNet	11	<b>16.5K</b>	303K	<b>4.93</b>	0.48px
	SuperPoint (5.5K)	11	7K	304K	4.93	0.81px
	D2-Net (12.5K)	11	<b>19K</b>	301K	3.03	1.40px
	R2D2 (12.6K)	11	13.4K	<b>308K</b>	5.02	1.47px
	Key.Net+HyNet (11.9K)	11	12.0K	307K	<b>7.81</b>	<b>0.69px</b>
<b>South Building 128 images</b>	SIFT (13.3K)	128	108K	<b>2.14M</b>	<b>6.04</b>	<b>0.54px</b>
	DoG+HardNet	128	159K	2.12M	5.18	0.62px
	DoG+SOSNet	128	160K	2.12M	5.17	0.63px
	DoG+HyNet	128	<b>166K</b>	2.12M	5.14	0.64px
	SuperPoint (10.6K)	128	125k	2.13M	7.10	0.83px
	D2-Net (12.4K)	128	<b>178K</b>	2.06M	3.11	1.36px
	R2D2 (13.2K)	128	136K	<b>3.31M</b>	5.60	1.43px
	Key.Net+HyNet (12.9K)	128	100K	2.11M	<b>12.03</b>	<b>0.74px</b>
<b>Madrid Metropolis 1344 images</b>	SIFT (7.4K)	500	116K	<b>1.82M</b>	<b>6.32</b>	<b>0.60px</b>
	DoG+HardNet	<b>697</b>	261K	1.27M	4.16	0.98px
	DoG+SOSNet	675	240K	1.27M	4.40	0.94px
	DoG+HyNet	<b>697</b>	<b>337K</b>	1.25M	3.93	0.98px
	SuperPoint (2.1K)	702	125K	1.14M	4.43	<b>1.05px</b>
	D2-Net (7.74K)	787	229K	0.96M	5.50	1.27px
	R2D2 (12.9K)	790	158K	1.15M	<b>7.26</b>	1.20px
	Key.Net+HyNet (9.3K)	<b>897</b>	<b>386K</b>	<b>1.62M</b>	5.87	<b>1.05px</b>
<b>Gendar- menmarkt 1463 images</b>	SIFT (8.5K)	1035	338K	<b>4.22M</b>	<b>5.52</b>	<b>0.69px</b>
	DoG+HardNet	1018	827K	2.06M	2.56	1.09px
	DoG+SOSNet	1129	729K	3.05M	3.85	0.95px
	DoG+HyNet	<b>1181</b>	<b>927K</b>	2.93M	3.49	1.05px
	SuperPoint (2.3K)	1112	236K	2.49M	4.74	<b>1.10px</b>
	D2-Net (8.0K)	1225	541K	2.60M	5.21	1.30px
	R2D2 (13.3K)	1226	529K	<b>3.80M</b>	<b>6.38</b>	1.21px
	Key.Net+HyNet (10.6K)	<b>1259</b>	<b>897K</b>	3.58M	5.79	1.13px

Table 2: Evaluation results on ETH dataset [36] for SfM. The improvement is in the number of registered images and sparse points, for large scenes in particular.

## 5 Discussion

In this section, we first investigate how each building block of HyNet contributes to the overall performance, then observe the impact of hyperparameters, and finally, we show the advantage of the proposed hybrid similarity measure over other possible solutions.

**Ablation Study** is presented in Table. 3, which shows how the  $L_2$  norm regularisation term  $R_{L_2}$ , similarity measure and feature map normalisation affect the performance. Specifically, we train different models on *Liberty* [5] and report average MAP on Hpatches [1] matching task. First, we can see that  $R_{L_2}$  helps to boost the performance, justifying our intuition that it optimises the network to be robust to illumination changes. Next, we experiment with different similarities for Eqn. (8), where the best results (through grid search for optimal margin) for each similarity are reported.

As shown,  $s_H$  improves from  $s_I$  and  $s_L$  by **1.87%** and **0.78%** respectively, indicating its effectiveness in balancing the gradient magnitude obtained from the positive and negative samples. Finally, Filter Response Normalisation (FRN) [39] is compared to Batch Normalisation (BN) [17] and Instance Normalisation(IN) [42], where the network with BN is commonly

Target	Choice	Other components	MAP
$R_{L_2}$	$\times$	FRN, $s_H$	53.58
	$\checkmark$	FRN, $s_H$	<b>53.97</b>
Similarity measure	$s_L$	FRN, $\checkmark R_{L_2}$	52.10
	$s_I$	FRN, $\checkmark R_{L_2}$	53.19
	$s_H$	FRN, $\checkmark R_{L_2}$	<b>53.97</b>
Norm type	BN	$s_H$ , $\checkmark R_{L_2}$	52.04
	IN	$s_H$ , $\checkmark R_{L_2}$	52.47
	FRN	$s_H$ , $\checkmark R_{L_2}$	<b>53.97</b>

Table 3: Ablation of HyNet’s components.

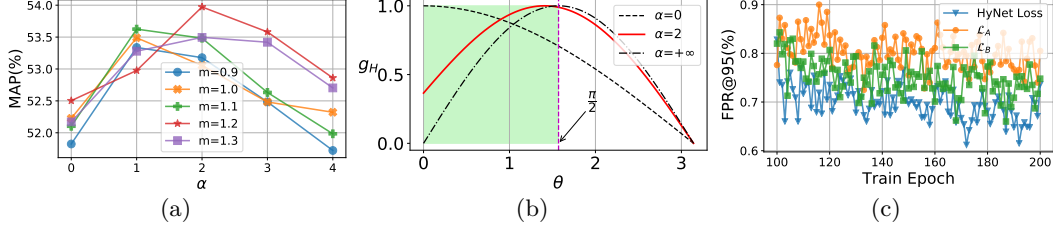


Figure 5: (a) Effect of parameter  $\alpha$  in the proposed hybrid loss. We give the matching MAP on HPatches [1] for different  $\alpha$  and margin  $m$  from Eqn. (7) and (8). (b) Gradient magnitude of the proposed HyNet loss for different  $\alpha$ . (c) Comparison of the proposed loss to other variants that combine the inner product and  $L_2$  loss.

used by previous methods [40, 26, 41, 15]. FRN surpass BN and IN by at least **1.5%**, which demonstrates the effectiveness of the affine  $L_2$  normalisation of the intermediate feature maps. Above all, by integrating  $R_{L_2}$ ,  $s_H$  and FRN together, we achieve the best result.

**Effect of  $\alpha$  and  $m$**  is investigated with grid search and reported in Fig. 5(a), where HyNet reaches top performance with  $\alpha = 2$  and  $m = 1.2$ . Furthermore, we denote  $g_H(\theta) = |\frac{ds_H(\theta)}{d\theta}|$  as the gradient magnitude for  $s_H(\theta)$ , and show its curve in Fig. 5(b). As seen, the curve of  $\alpha = 2$  is in between  $\alpha = +\infty$  for  $g_I(\theta)$  and  $\alpha = 0$  for  $g_L(\theta)$ , balancing the contributions from positives and negatives.

**Other possible solutions** for using different metrics for the positives and negatives include:

$$\begin{aligned}\mathcal{L}_A &= \frac{1}{N} \sum_{i=1}^N \max(0, m_{I,L} + s_I(\theta_i^+) - s_L(\theta_i^-)), \\ \mathcal{L}_B &= \frac{\alpha}{N} \sum_{i=1}^N \max(0, m_I + s_I(\theta_i^+) - s_I(\theta_i^-)) + \frac{1}{N} \sum_{i=1}^N \max(0, m_L + s_L(\theta_i^+) - s_L(\theta_i^-)).\end{aligned}\tag{10}$$

Specifically,  $\mathcal{L}_A$  uses  $s_I$  for positives while  $s_L$  for negatives, which is intuitively the most direct approach for adaptive gradient magnitude. Meanwhile,  $\mathcal{L}_B$  stacks two triplet losses, where  $m_I$  and  $m_L$  are the two margins. We conduct grid search for  $\mathcal{L}_A$  and  $\mathcal{L}_B$ , and set  $m_{I,L} = 1.0$ ,  $\alpha = 2.0$ ,  $m_I = 0.9$  and  $m_L = 1.2$ . Following [41], we compare their training curves with our HyNet loss in Fig. 5(c), where networks are trained on *Liberty* and FPR@95 are average on *Notredame* and *Yosemite*. As shown, our HyNet loss using  $s_H$  surpasses the other two solutions. Worth noting, that direct combination in  $\mathcal{L}_A$  does not show an advantage. We believe that the triplet loss with a linear margin does not fit well the nonlinear transformation between  $s_I$  and  $s_L$ , *i.e.*,  $s_L = \sqrt{2(1 - s_I)}$ , but we leave it for future investigation. Meanwhile, stacking triplet losses with different similarity measures is also sub-optimal, which further justifies the effectiveness of the proposed hybrid similarity.

## 6 Conclusion

We have introduced a new deep local descriptor named HyNet, which is inspired by the analysis and optimisation of the descriptor gradients. HyNet further benefits from a regularisation term that constrains the descriptor magnitude before  $L_2$  normalisation, a hybrid similarity measure that makes different contributions from positive and negative pairs, and a new network architecture which  $L_2$  normalises the intermediate feature maps. Empirically, HyNet outperforms previous methods by a significant margin on various tasks. Moreover, a comprehensive ablation study is conducted revealing the contribution of each proposed component on its final performance.



## References

- [1] Vassileios Balntas, Karel Lenc, Andrea Vedaldi, and Krystian Mikolajczyk. Hpatches: A benchmark and evaluation of handcrafted and learned local descriptors. In *Proceedings of the IEEE Conference on Computer Vision and Pattern Recognition (CVPR)*, volume 4, page 6, 2017.
- [2] Vassileios Balntas, Edgar Riba, Daniel Ponsa, and Krystian Mikolajczyk. Learning local feature descriptors with triplets and shallow convolutional neural networks. In *British Machine Vision Conference (BMVC)*, volume 1, page 3, 2016.
- [3] Axel Barroso-Laguna, Edgar Riba, Daniel Ponsa, and Krystian Mikolajczyk. Key.net: Keypoint detection by handcrafted and learned cnn filters. *Proceedings of the IEEE International Conference on Computer Vision*, 2019.
- [4] Eric Brachmann and Carsten Rother. Neural-guided ransac: Learning where to sample model hypotheses. In *Proceedings of the IEEE International Conference on Computer Vision (ICCV)*, pages 4322–4331, 2019.
- [5] Matthew Brown, Gang Hua, and Simon Winder. Discriminative learning of local image descriptors. *IEEE Transactions on Pattern Analysis and Machine Intelligence*, 33(1):43–57, 2011.
- [6] De Cheng, Yihong Gong, Sanping Zhou, Jinjun Wang, and Nanning Zheng. Person re-identification by multi-channel parts-based cnn with improved triplet loss function. In *Proceedings of the IEEE Conference on Computer Vision and Pattern Recognition (CVPR)*, pages 1335–1344, 2016.
- [7] Ondrej Chum, Tomas Werner, and Jiri Matas. Two-view geometry estimation unaffected by a dominant plane. In *Proceedings of the IEEE Conference on Computer Vision and Pattern Recognition (CVPR)*, 2005.
- [8] Jiankang Deng, Jia Guo, Niannan Xue, and Stefanos Zafeiriou. Arcface: Additive angular margin loss for deep face recognition. In *Proceedings of the IEEE Conference on Computer Vision and Pattern Recognition*, pages 4690–4699, 2019.
- [9] Daniel DeTone, Tomasz Malisiewicz, and Andrew Rabinovich. Superpoint: Self-supervised interest point detection and description. In *Proceedings of the IEEE Conference on Computer Vision and Pattern Recognition Workshops*, pages 224–236, 2018.
- [10] Mihai Dusmanu, Ignacio Rocco, Tomas Pajdla, Marc Pollefeys, Josef Sivic, Akihiko Torii, and Torsten Sattler. D2-Net: A Trainable CNN for Joint Detection and Description of Local Features. In *Proceedings of the IEEE Conference on Computer Vision and Pattern Recognition (CVPR)*, 2019.
- [11] Patrick Ebel, Anastasiia Mishchuk, Kwang Moo Yi, Pascal Fua, and Eduard Trulls. Beyond Cartesian Representations for Local Descriptors. In *Proceedings of the IEEE International Conference on Computer Vision (ICCV)*, 2019.
- [12] Weifeng Ge. Deep metric learning with hierarchical triplet loss. In *European Conference on Computer Vision (ECCV)*, pages 269–285, 2018.
- [13] Hugo Germain, Guillaume Bourmaud, and Vincent Lepetit. S2dnet: Learning accurate correspondences for sparse-to-dense feature matching. *arXiv preprint arXiv:2004.01673*, 2020.
- [14] Ian Goodfellow, Yoshua Bengio, and Aaron Courville. *Deep learning*. MIT press, 2016.
- [15] Kun He, Yan Lu, and Stan Sclaroff. Local descriptors optimized for average precision. In *Proceedings of the IEEE Conference on Computer Vision and Pattern Recognition (CVPR)*, pages 596–605, 2018.
- [16] Alexander Hermans, Lucas Beyer, and Bastian Leibe. In defense of the triplet loss for person re-identification. *arXiv preprint arXiv:1703.07737*, 2017.
- [17] Sergey Ioffe and Christian Szegedy. Batch normalization: Accelerating deep network training by reducing internal covariate shift. *arXiv preprint arXiv:1502.03167*, 2015.
- [18] Yuhe Jin, Dmytro Mishkin, Anastasiia Mishchuk, Jiri Matas, Pascal Fua, Kwang Moo Yi, and Eduard Trulls. Image matching across wide baselines: From paper to practice. *arXiv preprint arXiv:2003.01587*, 2020.

- [19] Michel Keller, Zetao Chen, Fabiola Maffra, Patrik Schmuck, and Margarita Chli. Learning deep descriptors with scale-aware triplet networks. In *Proceedings of the IEEE Conference on Computer Vision and Pattern Recognition (CVPR)*. IEEE, 2018.
- [20] Diederik P Kingma and Jimmy Ba. Adam: A method for stochastic optimization. *arXiv preprint arXiv:1412.6980*, 2014.
- [21] Hao Liu, Xiangyu Zhu, Zhen Lei, and Stan Z Li. Adaptiveface: Adaptive margin and sampling for face recognition. In *Proceedings of the IEEE Conference on Computer Vision and Pattern Recognition (CVPR)*, pages 11947–11956, 2019.
- [22] Yuan Liu, Zehong Shen, Zhixuan Lin, Sida Peng, Hujun Bao, and Xiaowei Zhou. Gift: Learning transformation-invariant dense visual descriptors via group cnns. In *Advances in Neural Information Processing Systems (NeurIPS)*, pages 6990–7001, 2019.
- [23] David G Lowe. Distinctive image features from scale-invariant keypoints. *Proceedings of the IEEE International Conference on Computer Vision (ICCV)*, 60(2):91–110, 2004.
- [24] Zixin Luo, Tianwei Shen, Lei Zhou, Siyu Zhu, Runze Zhang, Yao Yao, Tian Fang, and Long Quan. Geodesc: Learning local descriptors by integrating geometry constraints. In *European Conference on Computer Vision (ECCV)*, pages 170–185. Springer, 2018.
- [25] Zixin Luo, Lei Zhou, Xuyang Bai, Hongkai Chen, Jiahui Zhang, Yao Yao, Shiwei Li, Tian Fang, and Long Quan. Aslfeat: Learning local features of accurate shape and localization. *arXiv preprint arXiv:2003.10071*, 2020.
- [26] Anastasiia Mishchuk, Dmytro Mishkin, Filip Radenovic, and Jiri Matas. Working hard to know your neighbor’s margins: Local descriptor learning loss. In *Advances in Neural Information Processing Systems (NeurIPS)*, pages 4826–4837, 2017.
- [27] Kwang Moo Yi, Eduard Trulls, Yuki Ono, Vincent Lepetit, Mathieu Salzmann, and Pascal Fua. Learning to find good correspondences. In *Proceedings of the IEEE Conference on Computer Vision and Pattern Recognition (CVPR)*, pages 2666–2674, 2018.
- [28] Kevin Musgrave, Serge Belongie, and Ser-Nam Lim. A metric learning reality check. *arXiv preprint arXiv:2003.08505*, 2020.
- [29] Yuki Ono, Eduard Trulls, Pascal Fua, and Kwang Moo Yi. Lf-net: learning local features from images. In *Advances in Neural Information Processing Systems (NeurIPS)*, pages 6234–6244, 2018.
- [30] Omkar M Parkhi, Andrea Vedaldi, and Andrew Zisserman. Deep face recognition. In *BMVC*, 2015.
- [31] Adam Paszke, Sam Gross, Soumith Chintala, Gregory Chanan, Edward Yang, Zachary DeVito, Zeming Lin, Alban Desmaison, Luca Antiga, and Adam Lerer. Automatic differentiation in pytorch. In *NIPS-W*, 2017.
- [32] Jerome Revaud, Philippe Weinzaepfel, César De Souza, Noe Pion, Gabriela Csurka, Yann Cabon, and Martin Humenberger. R2d2: Repeatable and reliable detector and descriptor. *arXiv preprint arXiv:1906.06195*, 2019.
- [33] Ignacio Rocco, Relja Arandjelović, and Josef Sivic. Efficient neighbourhood consensus networks via submanifold sparse convolutions. *arXiv preprint arXiv:2004.10566*, 2020.
- [34] Ignacio Rocco, Mircea Cimpoi, Relja Arandjelović, Akihiko Torii, Tomas Pajdla, and Josef Sivic. Neighbourhood consensus networks. In *Advances in Neural Information Processing Systems (NeurIPS)*, pages 1651–1662, 2018.
- [35] Paul-Edouard Sarlin, Daniel DeTone, Tomasz Malisiewicz, and Andrew Rabinovich. Superglue: Learning feature matching with graph neural networks. *arXiv preprint arXiv:1911.11763*, 2019.
- [36] Johannes Lutz Schönberger, Hans Hardmeier, Torsten Sattler, and Marc Pollefeys. Comparative evaluation of hand-crafted and learned local features. In *Proceedings of the IEEE Conference on Computer Vision and Pattern Recognition (CVPR)*, 2017.
- [37] Florian Schroff, Dmitry Kalenichenko, and James Philbin. Facenet: A unified embedding for face recognition and clustering. In *Proceedings of the IEEE Conference on Computer Vision and Pattern Recognition (CVPR)*, pages 815–823, 2015.

- [38] Edgar Simo-Serra, Eduard Trulls, Luis Ferraz, Iasonas Kokkinos, Pascal Fua, and Francesc Moreno-Noguer. Discriminative learning of deep convolutional feature point descriptors. In *Proceedings of the IEEE International Conference on Computer Vision (ICCV)*, pages 118–126, 2015.
- [39] Saurabh Singh and Shankar Krishnan. Filter response normalization layer: Eliminating batch dependence in the training of deep neural networks. *arXiv preprint arXiv:1911.09737*, 2019.
- [40] Yurun Tian, Bin Fan, and Fuchao Wu. L2-net: Deep learning of discriminative patch descriptor in euclidean space. In *Proceedings of the IEEE Conference on Computer Vision and Pattern Recognition (CVPR)*, volume 1, page 6, 2017.
- [41] Yurun Tian, Xin Yu, Bin Fan, Fuchao Wu, Huub Heijnen, and Vassileios Balntas. Sosnet: Second order similarity regularization for local descriptor learning. In *Proceedings of the IEEE Conference on Computer Vision and Pattern Recognition (CVPR)*, pages 11016–11025, 2019.
- [42] Dmitry Ulyanov, Andrea Vedaldi, and Victor Lempitsky. Instance normalization: The missing ingredient for fast stylization. *arXiv preprint arXiv:1607.08022*, 2016.
- [43] Hao Wang, Yitong Wang, Zheng Zhou, Xing Ji, Dihong Gong, Jingchao Zhou, Zhifeng Li, and Wei Liu. Cosface: Large margin cosine loss for deep face recognition. In *Proceedings of the IEEE Conference on Computer Vision and Pattern Recognition*, pages 5265–5274, 2018.
- [44] Zhenhua Wang, Bin Fan, and Fuchao Wu. Local intensity order pattern for feature description. In *Proceedings of the IEEE International Conference on Computer Vision (ICCV)*, pages 603–610. IEEE, 2011.
- [45] Kwang Moo Yi, Eduard Trulls, Vincent Lepetit, and Pascal Fua. Lift: Learned invariant feature transform. In *European Conference on Computer Vision (ECCV)*, pages 467–483. Springer, 2016.
- [46] Baosheng Yu, Tongliang Liu, Mingming Gong, Changxing Ding, and Dacheng Tao. Correcting the triplet selection bias for triplet loss. In *European Conference on Computer Vision (ECCV)*, pages 71–87, 2018.
- [47] Linguang Zhang and Szymon Rusinkiewicz. Learning local descriptors with a cdf-based dynamic soft margin. In *Proceedings of the IEEE Conference on Computer Vision and Pattern Recognition (CVPR)*, pages 2969–2978, 2019.
- [48] Linguang Zhang and Szymon Rusinkiewicz. Learning local descriptors with a cdf-based dynamic soft margin. In *Proceedings of the IEEE International Conference on Computer Vision (ICCV)*, pages 2969–2978, 2019.
- [49] Xin-Yu Zhang, Le Zhang, Zao-Yi Zheng, Yun Liu, Jia-Wang Bian, and Ming-Ming Cheng. Adasample: Adaptive sampling of hard positives for descriptor learning. *arXiv preprint arXiv:1911.12110*, 2019.

## A Appendix

### A.1 Image Matching Challenge 2020

We further evaluate HyNet on the newly proposed Image Matching Challenge<sup>2</sup> (IMC) dataset [18]. It consists of two tasks, namely wide-baseline stereo and multi-view reconstruction. Since the ground truth for the test set is not released, we report the performance on the validation set. For fair comparison, we use Key.Net [3] as the detector and compare HyNet with two other state-of-the-art descriptors, HardNet [26] and SOSNet [41]. The evaluation protocol is with a maximum of 2048 keypoints per image and standard descriptor size (512 bytes). We use DEGENSAC [7] for geometric verification, and nearest-neighbour matcher with first-to-second nearest-neighbour ratio test for filtering false-positive matches. Please refer to [18] for exact details of the challenge’s settings.

	mAA (%)		
	Stereo	Multi-View	Average
HardNet [26]	63.40	74.41	68.91
SOSNet [41]	63.41	74.51	68.96
HyNet	<b>64.07</b>	<b>74.84</b>	<b>69.46</b>

Table 4: Mean Average Accuracy (mAA) at 10° on IMC dataset [18].

As can be seen from Table 4, HyNet surpasses the previous state-of-the-art methods HardNet and SOSNet on both tasks, which further validates its effectiveness.

### A.2 Integrating HyNet with SOSR

In this section, we test HyNet by combining it with the Second Order Similarity Regularisation (SOSR) proposed in [41], results are shown in Table 5 and Fig. 6. As shown, HyNet generalises well with the extra supervision signal from SOSR, indicating its potential of being further boosted by other third-party loss terms.

Train	ND	YOS	LIB	YOS	LIB	ND	Mean
Test	LIB		ND		YOS		
SIFT [23]	29.84		22.53		27.29		26.55
HardNet [26]	1.49	2.51	0.53	0.78	1.96	1.84	1.51
SOSNet [41]	1.08	2.12	0.35	0.67	1.03	0.95	1.03
HyNet	<b>0.89</b>	<b>1.37</b>	0.34	0.61	0.88	0.96	0.84
HyNet+SOSR [41]	0.91	1.62	<b>0.31</b>	<b>0.54</b>	<b>0.78</b>	<b>0.73</b>	<b>0.82</b>

Table 5: Patch verification performance on the UBC phototour dataset. Numbers denote false positive rates at 95% recall(FPR@95). ND: Notredame, LIB: Liberty, YOS: Yosemite.

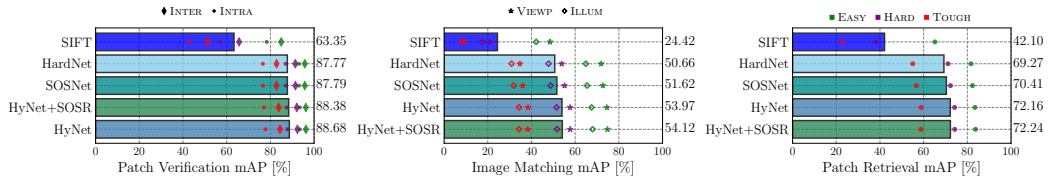


Figure 6: Results on test set ‘a’ of HPatches [1]. Colour of the marker indicates EASY, HARD, and TOUGH noise. The type of marker corresponds to the variants of the experimental settings.

<sup>2</sup><https://vision.uvic.ca/image-matching-challenge/benchmark/>